Experimental and Numerical Analysis of the Failure of Notched Concrete Beams

F. Antico, I. De la Varga, M. Pour-Ghaz

Purdue University, School of Civil Engineering, West Lafayette, IN, 47907

ABSTRACT: The main objective of the present work is to study the effect of material properties on the failure of the concrete samples under three point bending test. In the present study experimental and numerical methods were used to study the failure of the notched beam concrete specimens under three point bending. Three different aggregate types were used to make different concrete specimens (normal weight river sand, expanded clay porous light weight aggregate, and Styrofoam inclusions). Tests to obtain the tensile strength and the elastic modulus of the specimens were carried out. These values were used as inputs for the numerical simulation. In addition, load-displacement and load-crack mouth opening displacement (CMOD) plots were obtained experimentally and correlated with numerical results. Numerical simulations included two-dimensional modeling of the three point bending test using finite element method.

The experimental results showed that the tensile strength of the concrete containing Styrofoam particles was the lowest, whereas the normal weight concrete sample (concrete with normal weight aggregate) depicted the highest value. This is consistent with the results obtained from the simulation. However, the trend and values obtained from the three point bending test were not comparable with those from the simulation.

1. BACKGROUND

The fracture behavior of the cement-based composites is sensitive to the type of aggregates and the aggregate-cement paste interface. Inclusion of different type of aggregates can modify the fracture properties of cement-based materials. In the present study three types of inclusions were used in cement-based composites to modify the fracture properties of these composites. The first type of inclusion was the normal weight river sand which is used in conventional concrete materials. The second type of inclusion was porous light weight aggregate. This type of aggregate is made by high temperature burning of clay. Since this type of inclusion is highly porous it holds a significant amount of water. This extra water improves the reaction of cement paste at the interface of the inclusion and cement-paste matrix (also known as interfacial transition zone (ITZ)). This improvement enhance the fracture properties of the composite. The opposing effect however is that the light weight aggregate is a porous material.

In general, the mechanical response of concrete or mortar specimens loaded in three point bending configuration can be analyze using an appropriate model to predict the pre-peak, peak load, and softening behavior before collapse. For this purposes, previous investigations presented analytical models based on linear elastic fracture mechanics (LEFM) theory [1] assuming cement-based specimens as homogeneous materials. In terms of the modeling of the damage zone it was demonstrate that under specific conditions cement-based beams could present localized regions where damage occurs [2]. In relation to this, many investigations developed numerical models to represent the damage of mortars and concrete based on cohesive-zone-models [3-5]. Moreover, experimental techniques and simple theoretical models allow to characterize the properties of the FPZ of concrete beams by means of the change of stiffness due to the crack growth [6]. These and more recent investigations based on new techniques to visualize the damage of materials [5] are helping to explain the mechanisms of failure of this kind of materials.

The third type of concrete that was used in this work is prepared using zero-stiffness particles (Styrofoam). These particles replaced a part of the fine normal weight aggregate. These particles affect the strength and elastic properties of the composite. However, the spherical shape of these particles can contribute to the toughness by decrease the sharpness of the crack that is absorbed by these inclusions.

2. OBJECTIVES AND APPROACH

The main objective of this study is to evaluate the effect of material (i.e. concrete) properties on the fracture behavior. In this study the material properties is modified by changing the type of inclusions. Three different concretes were prepared and tested in a three-point bending set up. To better understand the effect of material properties numerical simulations were employed.

3. MATERIALS DESCRIPTION

An ordinary Portland cement (Type I) was used in this study. Both fine and coarse aggregates consisted of normal weight river sand and gravel respectively. These three components were mixed in a conventional concrete mixer in accordance with the procedure described in ASTM C192 [7]. This concrete was used as reference or plain concrete for comparison purposes. The second concrete type was with the same concrete mixture, however part of the fine aggregate was replaced with a fine light weight aggregate (LWA). LWA consists of a very porous material that is previously soaked in water during 24 h and used in concrete as internal curing agent. This means that LWA will provide that additional water at an appropriate time (i.e. after concrete sets) without modifying the water-to-cement ratio (*w/c*). Finally, the third type of concrete was prepared using zero-stiffness particles (Styrofoam). These particles replaced part of the fine normal weight aggregate (3.3 % by volume). All concrete specimens had a *w/c* of 0.36 and 55 % of aggregate (by volume). Table 1 shows the mixture designs to better observe the differences in the three types of concrete:

Table 1: Mixture Proportions

Mortar Mixture	Plain	LWA	EPS
Volume Fraction of Aggregate, %	55	55	55
water/cement (w/c)	0.36	0.36	0.36
Cement, kg/m^3	516	516	516
Water, kg/m^3	190	190	190
Fine Aggregate, kg/m^3	774	404	637
Coarse Aggregate, kg/m^3	962	962	962
LWA, kg/m^3	0	208	0
EPS, g/m^3	0	0	90
HRWRA, g/100g cementitious material	0.8	0.8	0.8

1 Kg/m^3 = 1.69 lb/yd^3

4. EXPERIMENTAL APPROACH

The experimental part of the study can be divided into two different experiments. In the first experiment the bulk materials properties such as elastic modulus and tensile strength were evaluated. These properties were used to run numerical simulations. In the second part of the experimental program, three-point bending test was used.

Experiment 1: Inputs values for FEM simulation

Since the main objective of this study is to compare experimental results with numerical simulations, some material properties needed as input values for the simulation are taken from experiments. All concretes were cured during 14 days, age at which all the parameters were measured. These values are:

- Density: Taken from mixture proportions (see Table 1).
- Tensile strength: Experiment performed on 4 x 8 inch concrete cylinders according to ASTM C496, also known as 'Brazilian Test'.
- Modulus of elasticity: Experiment performed on 4 x 8 inch concrete cylinders according to ASTM C469.
- Compressive strength: Data obtained from previous studies. The same strength was assumed in all three concretes.
- Critical crack mouth opening displacement ($CMOD_c$): Approximation obtained from John and Shah [8] as a function of the compressive strength. Equation 6 shows the empirical equation.

Experiment 2: Three-point bending test

Beam concrete specimens with dimensions of 3 x 3 x 15 inches were prepared for this part of the study. The beams were tested in a universal testing machine (UTM). Two linear variable differential transducers (LVDT) were used to measure both vertical (i.e. machine) and horizontal (i.e. crack opening) displacements. These parameters were used to generate load-displacement and load-CMOD plots that were compared with the results obtained by the FEM simulation. Figure 1 shows the set up of this test. The span of the beam during loading was 13 inches. Teflon was used at all contact points between the loading frame and the sample to reduce frictional effects.

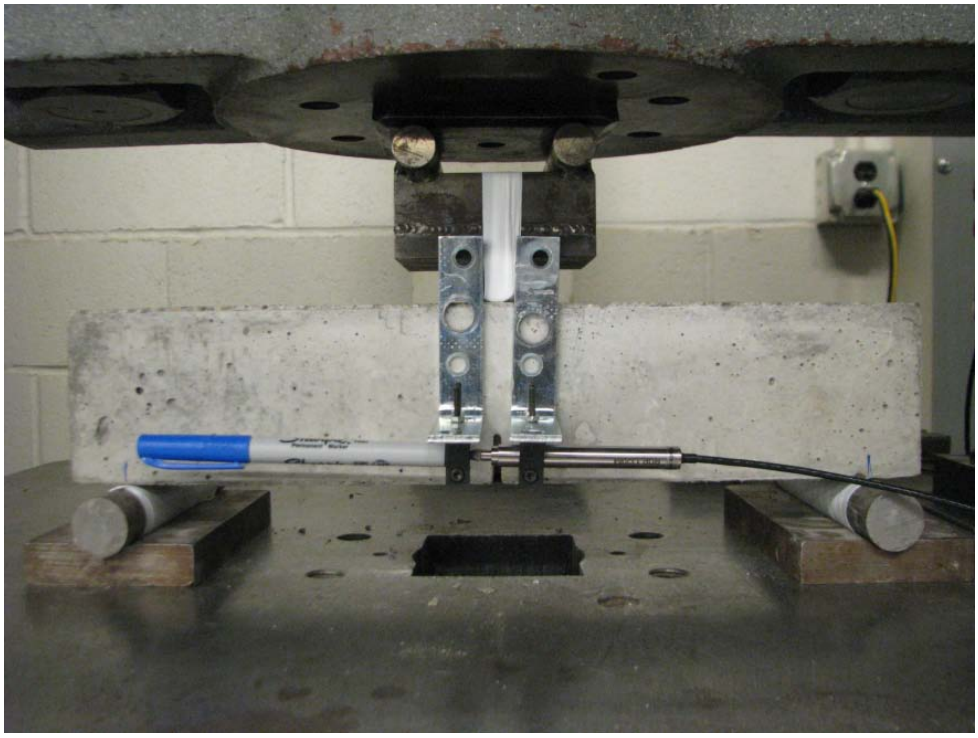

Figure 1 Three point bending set up

5. NUMERICAL MODELING

The purpose of this section is to present the theoretical background of the finite element model (*FEM*) developed for this investigation to understand and represent the mechanical response of early-age-concrete-beams under quasi-static loading condition. Two approaches are followed in this investigation. The first approach is based on experimental data provided by Brazilian tests performed for this investigation and previous investigations. The second approach is a parametric study to understand, qualitatively, how fractures properties defined in the CZM are related to the mechanical response of concrete samples in three point bending configuration.

A *2D* plain-strain model is proposed to represent the mechanical behavior of mortars in three point bending configuration. The bulk material is represented by a 4-noded-quadrilateral-elements mesh. The modeling is completed by the implementation of cohesive elements in line configuration in the central region of the beam that allow representing the softening behavior once the damage has started. Figure 2 shows the schematics of the numerical model. Simply support condition is defined as boundary condition and the load is applied in a displacement control fashion to match the conditions of the experiments.

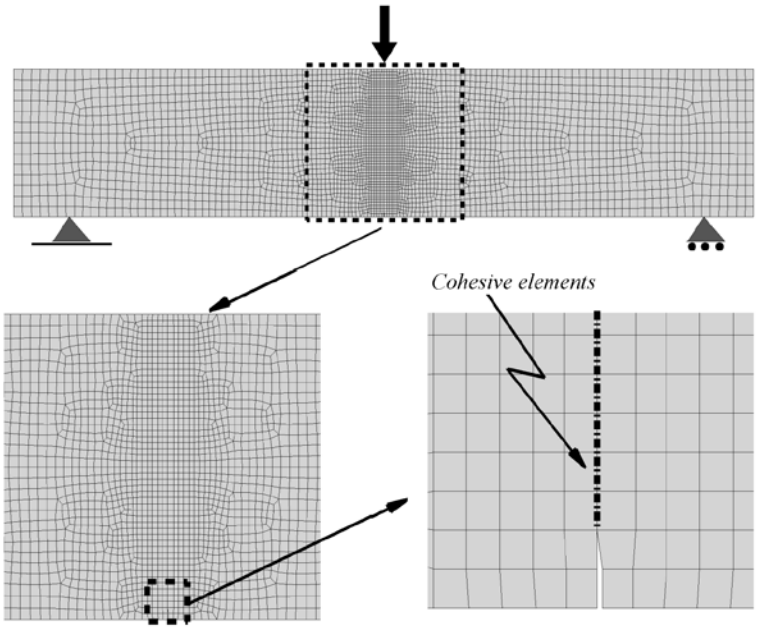

Figure 2 Scheme of the mesh used for the simulations. In the details it is shown the region where the cohesive elements were embedded.

It is assumed that the bulk material behaves as a linear elastic material. As presented in previous sections, the mechanical properties of the different kinds of concretes were obtained experimentally by the implementation of Brazilian's test. Young's modulus (*E*), Poisson ratio (ν) and density (ρ) were used to define the properties of the bulk. Also, it was observed during the tests that the samples presented small deformations and rotations prior to the complete failure. Even thought, it could be expected that large rotations occur close to the collapse of the samples. Then, the *FEM* was set to take into account large rotations. The simulations are solved using and explicit scheme. Therefore, to assure that the simulation represents a monotonic quasi-static loading condition, a convergence test is performed to verify that inertia effects can be neglected. Based on this analysis, the selected rate of loading for the simulations is set around to 0.022 mph. Figure 3 shows the response of the model in terms of the force and displacement measured in the point where the external displacement is applied.

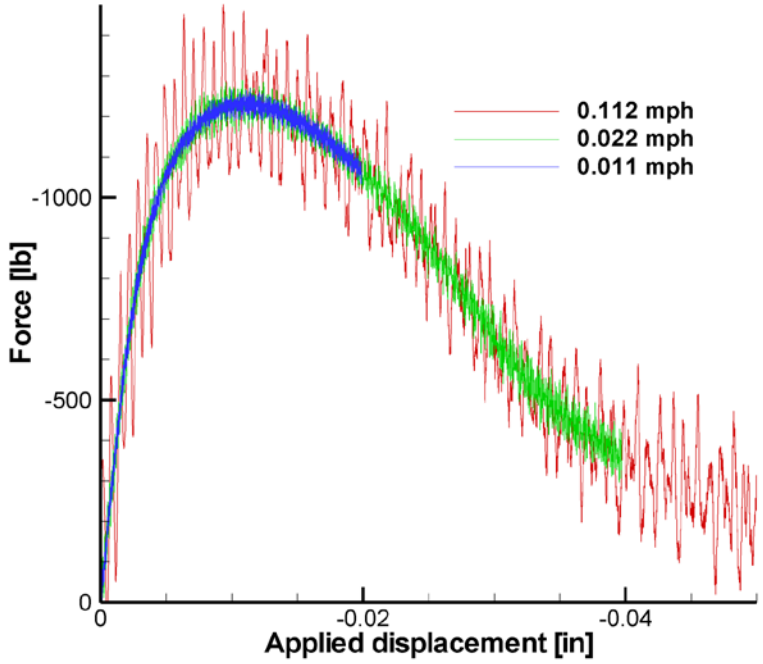

Figure 3 Convergence test done to set up the dynamic parameters of the simulation. The oscillation that is observed corresponds to the geometrical and dynamic properties of the solid. In a lower scale (not in this picture) it is possible to see the oscillations related with FEM.

As mentioned before, the central line of the mortar is modeled with a cohesive zone model [9-13] to simulate crack initiation and propagation. The model takes into account an initial crack of approximately one inch to match the experiments. A potential-based law cohesive zone model implemented as triangular-shape four-node zero-thickness interface elements [14] is embedded between the bulk elements of the mortar. The formulation of these elements is based on a non-dimensional effective displacement jump (λ) that takes into account the current normal and tangential displacement jumps at the interface estimated by the finite element analysis.

$$\lambda = \sqrt{\left(\frac{u_n}{\delta_n}\right)^2 + \xi^2 \left(\frac{u_n}{\delta_n}\right)^2} \qquad (1)$$

where, u_n and u_t are the current normal and tangential displacement jumps at the interface estimated by the finite element analysis, δ_n and δ_t are the critical values of the displacement jump at which interface failure takes place.

During the finite element calculation, the displacement jump is related with the strength of the interface using a traction separation law as defined in [14] for mode I and mode II

$$T_n = \frac{1-\lambda^*}{\lambda^*}\left(\frac{u_n}{\delta_n}\right)\frac{T_{max}}{(1-\lambda_{cr})} \quad (2)$$

$$T_t = \frac{1-\lambda^*}{\lambda^*}\left(\frac{u_t}{\delta_t}\right)\frac{\alpha T_{max}}{(1-\lambda_{cr})} \quad (3)$$

where λ^* is monotonically increased by

$$\lambda^* = \max(\lambda_{max}, \lambda) \quad (4)$$

where, $\lambda_{max} = \lambda_{cr}$ initially and $\lambda_{max} = \lambda$ if $\lambda > \lambda_{max}$. Also, in these equations, T_{max} is the cohesive strength of the interface in the normal direction, and $\alpha T_{max} = \tau_{max}$, the strength in the tangential direction. Then, the values of δ_n and δ_t could be derived from the geometrical relation of the strength and the cohesive energy (fracture energy) of the interface

$$G_{Ic} = \frac{1}{2}\delta_n T_{max}, \quad G_{IIc} = \frac{1}{2}\delta_t \alpha T_{max} \quad (5)$$

The strength and energy of the cohesive zone in the numerical model are studied and defined based on the information of the tests performed for this investigation. Figure 4 shows the cohesive traction-separation law for normal mode. Although the material properties of the mortar is known the specific cohesive parameters described in Eqs. 1-5 need to be identified accordingly. Another important feature for the interpretation of damage models is the fracture process zone length,l_f, usually estimated as $l_f \propto G_c E/T_{max}^2$ [15-17]. In our numerical investigation, we carry out a parametric analysis of the variation of the main cohesive parameters,T_{max}, G_c, δ_n. Then, the cohesive zone model can be determined by the definition of two of these parameters.

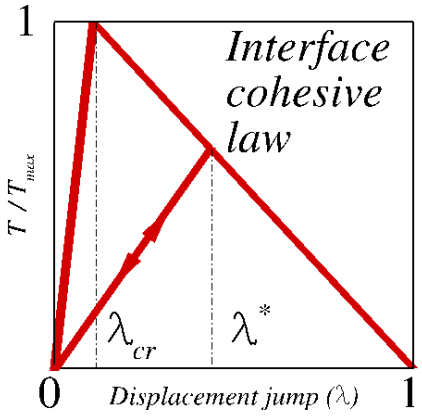

Figure 4 Triangular cohesive law used to represent the damage in mortar specimens. It is shown as an example the irreversible response of the model if the system is unloaded after the peak is reached.

It is worthy to mention that it was assumed the same cohesive properties for mode I and II (i.e. $\delta_n = \delta_t$ and $\alpha = 1$ to limit our analysis to only two main parameters, namely, $T_{max} = \sigma_{max}$ and $G_c = G_{IIc} = \frac{1}{2}\delta_t T_{max}$.

6. RESULTS AND DISCUSSIONS

a. Experimental Results

i. Experiment 1: bulk properties

Table 2 shows the results of the first set of experiments. Reported values in this table are obtained using the experiments described in previous sections. It can be seen that by addition of LWA and Styrofoam materials in concrete the elastic modulus and tensile strength decreases significantly.

Table 2: Experimentally obtained materials properties

	Plain Concrete	LWA Concrete	Styrofoam Concrete
Elastic Modulus (ksi)	5270	4627	3714
Density (lb/ft^3)	144	144	144
Tensile Strength (psi)	825	663	531
Compressive Strength (psi)	6700	6700	6700
CTOD (in.)	4x10^{-5}	4x10^{-5}	4x10^{-5}

ii. Experiment 2: Three point bending

Figure 5 shows a photograph of the beam before failure. As it can be seen in this figure a crack is observed before failure beam. In all sample a stable crack growth was observed before complete failure of the beam. Figure 6 illustrates the results of the three-point bending test. Figure 6a illustrates the load-displacement curve and Figure 6b illustrates the load-CMOD curve. It can be seen in both figure that the maximum peak load is observed for plain concrete. Concrete containing Styrofoam shows a higher toughness and strength compared to the LWA concrete.

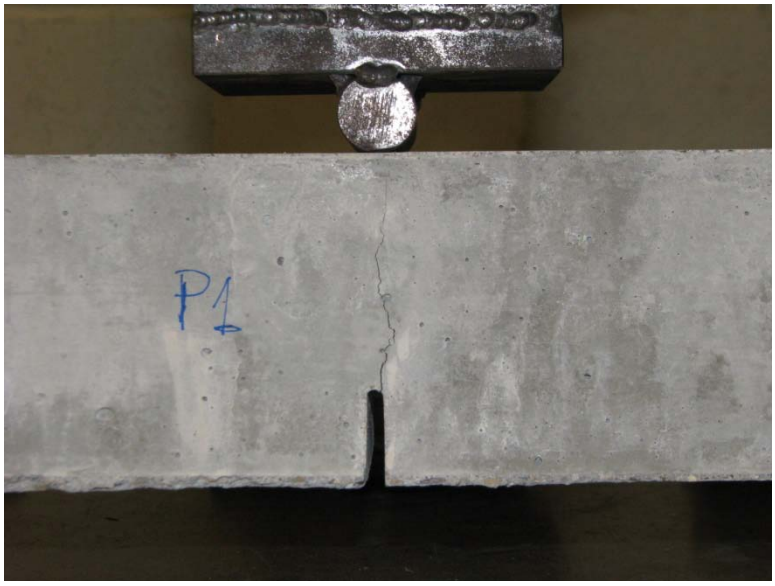

Figure 5 Beam before failure

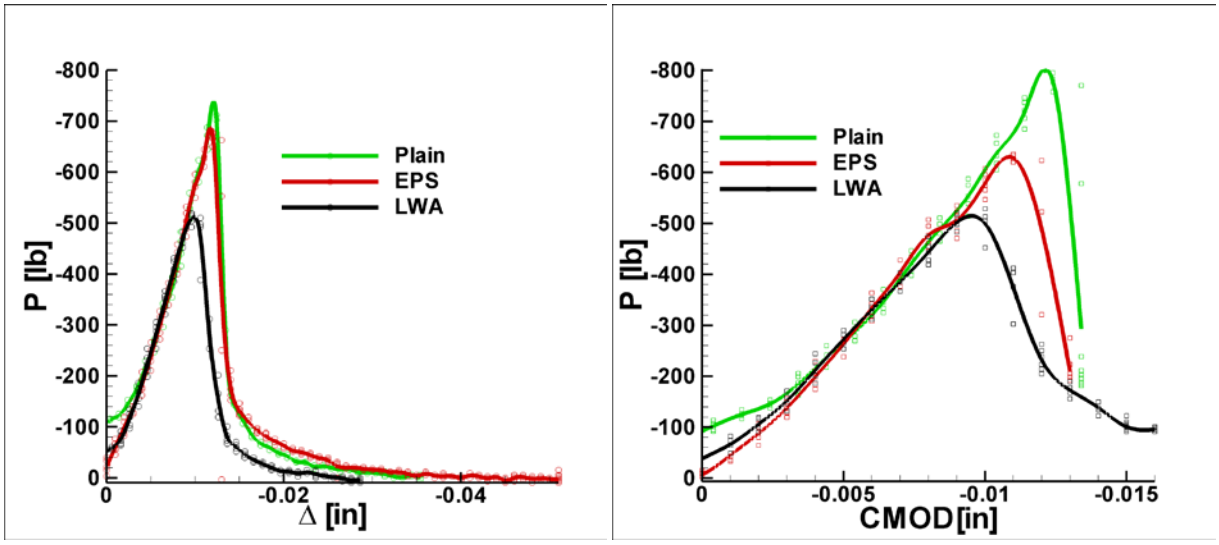

Figure 6 a) Load-displacement b) Load-CMOD

b. Numerical Results

i. Approach considering T_{max} and CTODc:

This approach is based on the definition of the tensile strength and *CTODc* from experiments. Unfortunately, it was not possible to capture the pre-peak behavior of the crack mouth opening displacement (*CMOD*) to get an estimation of the critical tip opening displacement (*CTODc*). Then, *CTODc* is estimated based on an empirical expression [fca.16] for high strength concrete (*HSC*)

$$CTODc = 0.00602(f'c)^{0.13} \quad (6)$$

where $f'c$ is the compressive strength of the material expressed in [MPa] to obtain *CTODc* in [millimeters]. The CTOD can be defined as the displacement at tip of the notch. Initially, and up some load level, the crack does not grow from the notch an the CTOD is zero. It is assumed that the response in this range is linearly elastic. Beyond this range, an intermediate stage occurs where the process zone is starting to develop and some separation occurs (CTOD > 0). Then, the structural response becomes non-linear. Following this the peak load is reached and the value of the load starts to decrease. Here CTODc is the critical CTOD.

Assuming that $f'c$ do not change for none of the material compositions of this investigation, is is assumed that *CTODc ~3.94e-4 in*. It is necessary to clarify that this empirical approximation may not be an accurate estimation of the critical tip opening for this investigation. The reason for this is that cement-based mortars (in general: Portland cement and sand) have a different microstructure composition compared with high strength concrete (in general: Portland cement, sand and aggregate) and then the composition, sizes of its constituents can lead to different mechanisms of failure. Also, the curing conditions may not be related between this specimen's investigation and the ones that were used to develop the empirical formulation.

The following table shows the input values of the CZM used on this approach. To do the numerical calculations the values tensile strength for one standard deviation below (LB) and above (UB) the mean value were selected as reference cases. E, ν and ρ are kept the constant for each type of material.

	$T_{max}\ [PSI]$	$G_{Ic}\ [\frac{lb}{in}]$
Plain (LB)	707.78	1.36E-01
Plain (UB)	941.29	1.81E-01
LWA (LB)	619.31	1.19E-01
LWA (UB)	706.33	1.36E-01
EPS (LB)	491.68	9.44E-02
EPS (UB)	570	1.09E-01

Table 3 Input values for the CZM for the first approach

The size of the FPZ (l_{fpz}) goes from 1.7 to 2.3 inches for these calculations. The values of l_{fpz} indicates that neither a *LEFM* nor engineering approach may be suitable to characterize the behavior

of the samples (size effect interpretation based on the geometrical and mechanical properties of the system).

Figure 7 shows a comparative of peak load values obtained from experiments and simulations based on this approach. The numerical results follow the trend impose by the tensile strength for each material. However, this trend is not follow by the results obtained from the three point bending test.

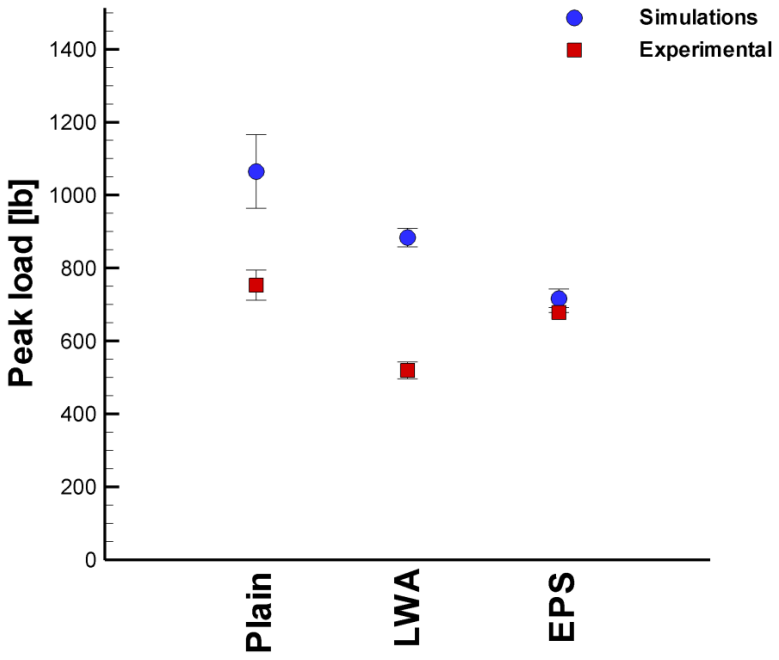

Figure 7 Comparison of numerical and experimental results of the peak load for each type of material.

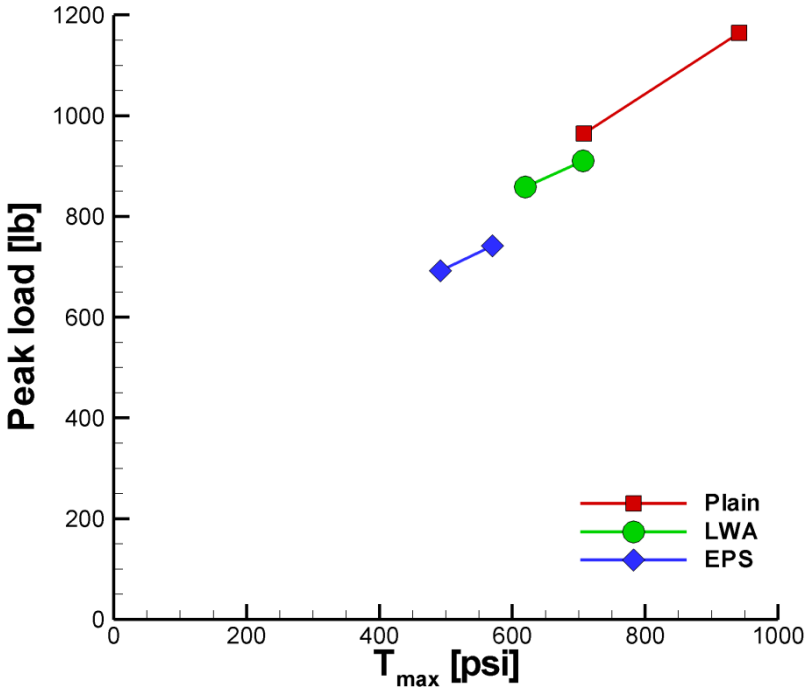

Figure 8 Numerical estimations of the peak load vs. the tensile strength obtained from experiments.

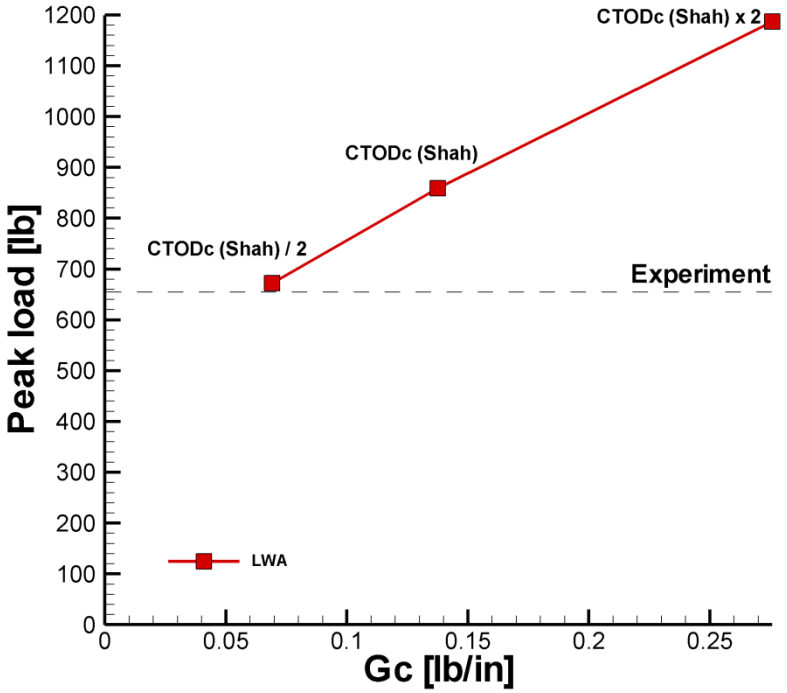

Figure 9 Parametric analysis of the peak load in terms of values of fracture energy for LWA. The reference case is set based on the empirical calculation of the CTODc. As a reference, the peak load of the three point bending experiment is indicated as a dashed line.

A parametric study of the model is presented to analyze the trend of the peak load in terms of changes of the tensile strength and *CTODc* (or *Gc*). Figure 8 shows the correlation made for the different values of the peak load according the type of material versus the characteristic tensile strength obtained from tests. The trend shows that the peak load increased with the increment of tensile strength. Figure 9 shows the correlation between the peak load and different values of energy for *LWA* as an example. The central value of the plot corresponds to the peak load obtained considering the empirical calculation of *CTODc* [18]. Two more cases assuming half and double of empirical CTODc are presented. The value of the peak load is also dependent on the second parameter of the cohesive zone model as it is expected from size effect interpretation.

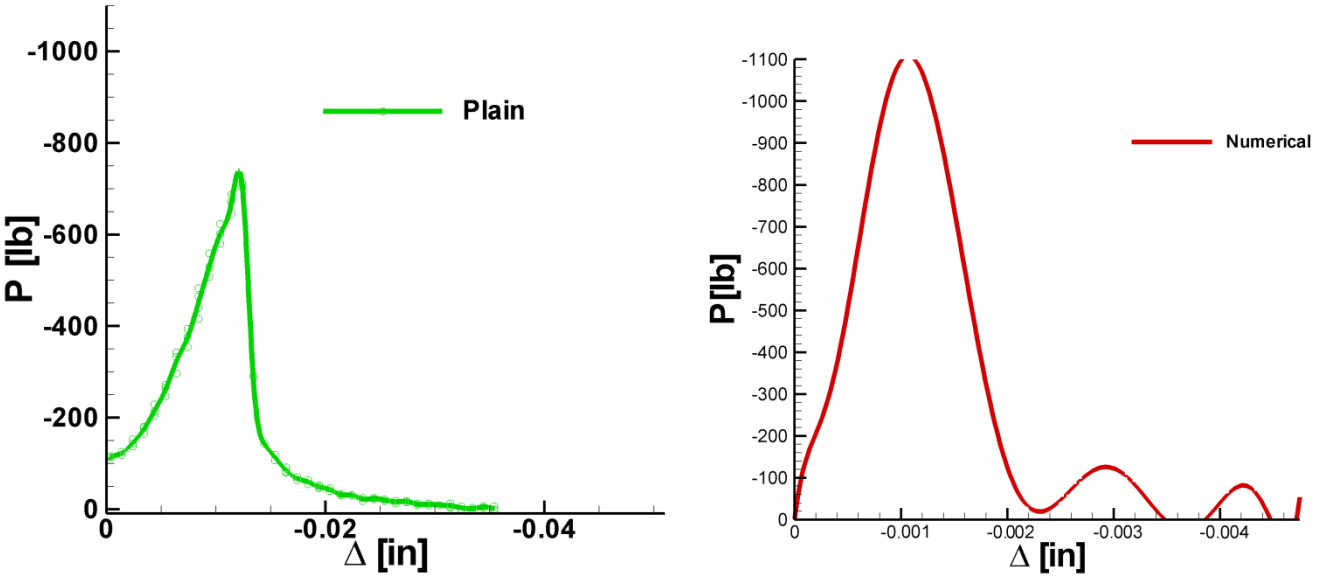

Figure 10 Comparative of Force vs. applied displacement obtained from experiements (Plain) and simulations. The CZM parameters were defined in terms of the tensile strength, obtained from Brazilian tests, and the critical displacement, defined by the an empirical estimation used for HSC.

Regardless of the fact that the numerical model and experiments presents good correlation of the peak load, the applied displacement predicted by simulations is an order of magnitude different. This difference is related to an inaccurate estimation of the fracture energy by the use of the empirical formula for *HSC*. Figure 10 shows the differences between experiments (e.g. Plain test) and simulations. The following approach will present a more exhaustive parametric analysis of the CZM's properties.

ii. Parametric study of T_{max} , G_c and E:

To complete this numerical analysis, a qualitative study is performed to identify the effects of the variation of tensile strength, fracture energy and Young's modulus in the response of the three point bending simulation. In the previous analysis it was observed that the proposed estimation of *CTODc* is not accurate for this type of materials. As said before, the values of *CTODc* can be related with the fracture energy of the material. We will refer to G_c and T_{max} based on metric units since most of the literature expresses this parameter in this format.

The obtained values of *CTODc* are related with a range of fracture energy between $16.8 < G_c < 32.2\ N/m$. A brief literature review showed that cement-based mortar specimens present values of fracture energy that goes from $60\ N/m$ [3] to values of $125\ N/m$ [18]. In terms of the tensile strength, the values obtained from Brazilian's test seem to match with the literature in general [3].

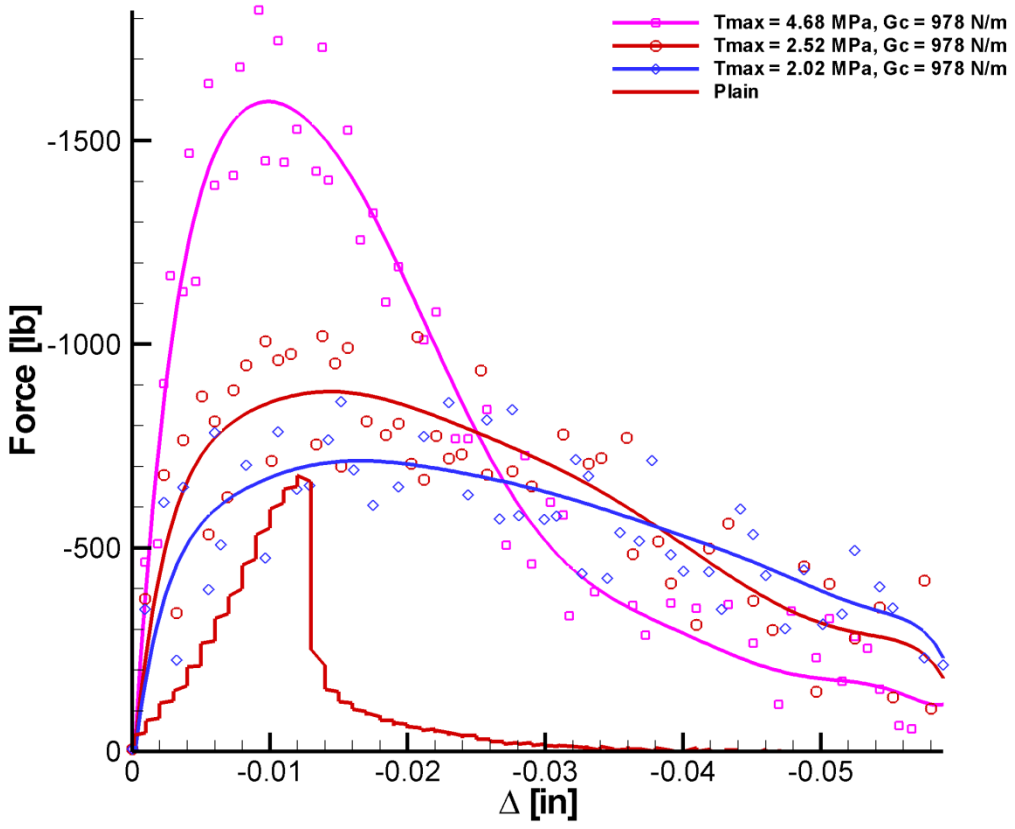

Figure 11 Parametric analysis of the tensile strength values used in the three point bending simulations.

The parametric analysis performed to evaluate the effects of changes of the tensile strength

are showed in Figure 11. This plot shows that changes in tensile strength for assuming fracture energy constant mainly affect the absolute value of the peak load. In this case it is observed that our simulations predicted that the samples tested in this investigation should be close $T_{max} = 2\ MPa$ (plain samples results were taken as an example). It is worthy to mention that Brazilian tests indicate that tensile strength for plain samples is around $4.5 < T_{max} < 6.9\ MPa$.

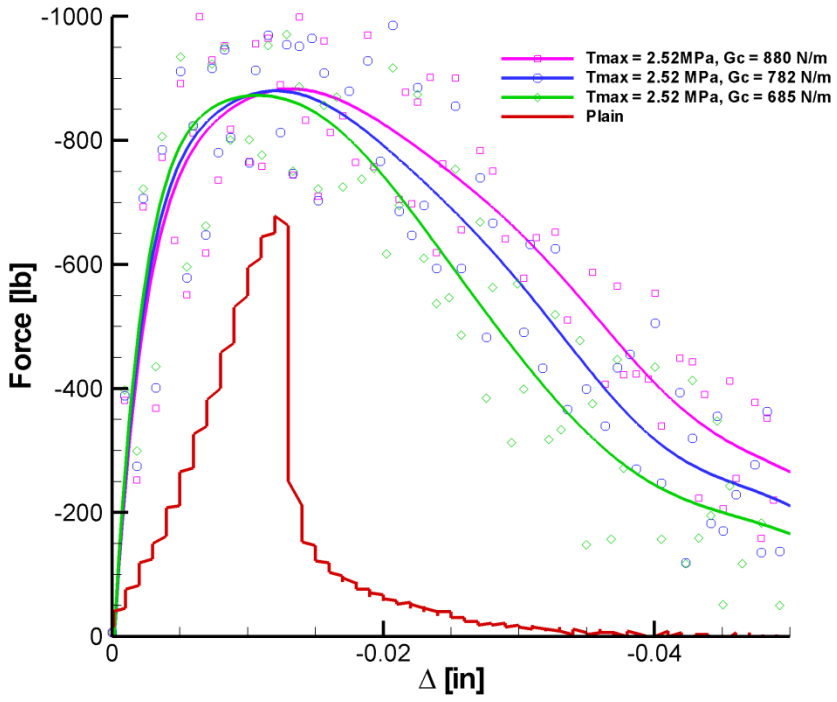

Figure 12 Parametric analysis of the fracture energy values used in the three point bending simulations.

On the other hand, Figure 12 shows the effect of changes in fracture energy assuming a constant value of tensile strength. From this figure, it is clear that changes in G_c mainly affects the post peak behabior. The values of G_c adopted for this parametric study are higher than the ones that probably represent the real post peak behavior. However, it is clear that the values G_c obtained based on the selected empirical formula are not suitable for this investigation. Assuming that the tensile strength and the Young's modulus are almost the same as the one obtained from experiments, it is possible to determine the size of the FPZ in terms of the G_c. For the values of energy presented in Figure 12, the estimated size of the FPZ is around $197 < l_{fpz} < 256\ in$.

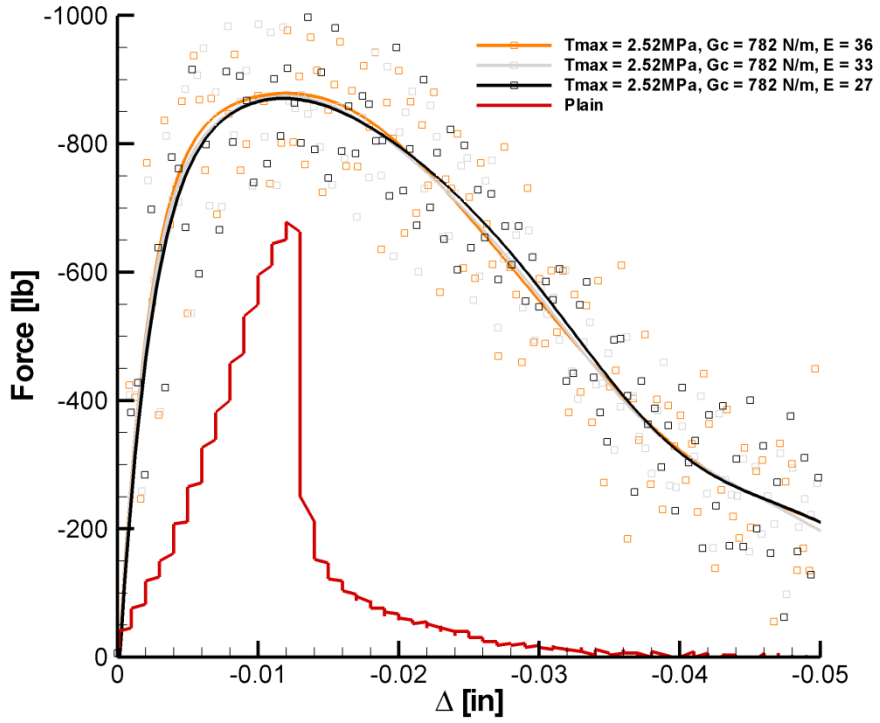

Figure 13 Parametric analysis of the Young's modulus values used in the three point bending simulations.

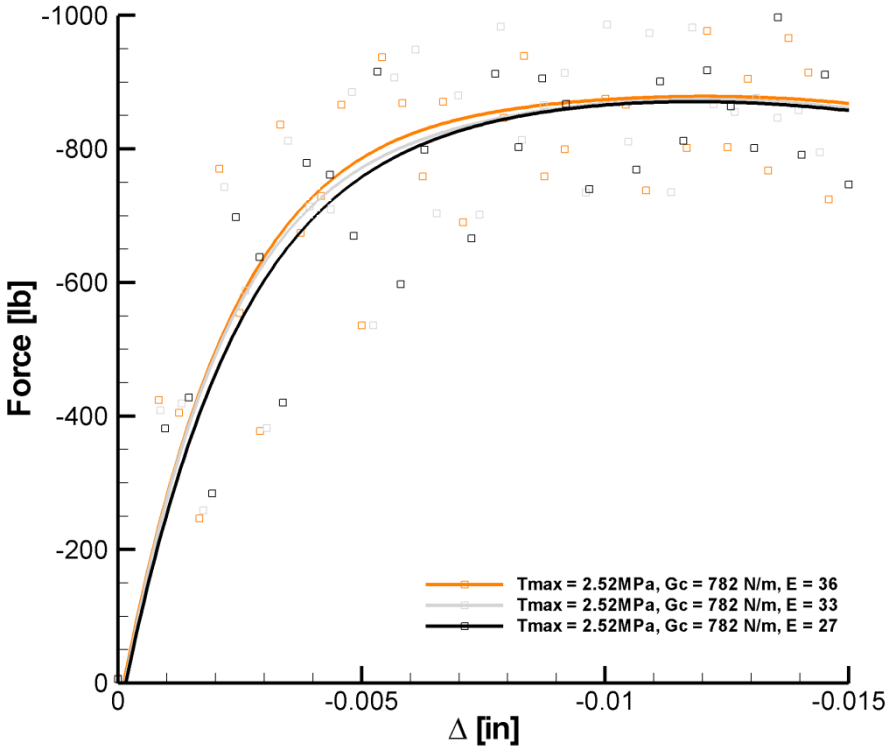

Figure 14 Detail of the pre-peak region of Figure 13.

Finally, we are also interested in the parametric analysis of the Young's modulus (*E*) which mainly affects the pre-peak behavior. Figure 13 and Figure 14 show that *E* does not affect the post peak behavior. On the contrary, changes in *E* affect the slope of the pre-peak response (see Figure 14), as expected.

7. CONCLUSIONS

The numerical part of this investigation developed a finite element model (FEM) to understand and represent the mechanical response of early-age-concrete-beams under quasi-static loading condition using a CZM model. As it was expected, CZM is suitable to represent the mechanical behavior of cement-based concretes. In relation to this model, it was verified that the mechanical response of the specimens is sensitive to both tensile strength and fracture energy. This means that neither LEFM nor engineering approach may be suitable to describe the response of these cement-based concretes. This could be also explained from the size-effect point of view. The size of the FPZ estimated using the equation proposed by Rice [17] is comparable with the dimensions of the specimens. For the estimations of this work, the size of the FPZ is of the same order of magnitude (model based on T_{max} and CTODc) or much larger (parametric analysis of T_{max}, G_c, E) than the characterirstic dimension of the specimens. Then, the results of the present investigation indicate that it is expected that real values of G_c would be between $32.2 < G_c < 685\ N/m$ - $58.4\ (2.3) < l_{fpz} < 500\ mm\ (197\ in)$, assuming $2 < T_{max} < 7\ MPa$.

This work allowed the authors to understand and refine the experimental, numerical techniques and assumptions needed to evaluate the mechanical response of early-age cement-based mortar beams. Moreover, the numerical results showed that it is possible to reproduce the trend observed during the experiments. However, more work is needed to obtain an accurate estimation of the parameters that represents the overall behavior of these mortar beams. In future works more realistic approximations of the fracture energy would be obtained by the implementation of a bi-linear cohesive [19] to improve the modeling of the post-peak behavior.

8. REFERENCES

[1] Wecharatana, Shah, “Predictions of nonlinear fracture process zone in concrete”. *Journal of Engineering Mechanics*, 109(5), 1983.

[2] Z.Bazant, “Identification of strain-softening constitutive relation from uniaxial test by series coupling model for localization”, *CCR*, 19, pp.973-977, 1989

[3] G.Ruiz, M. Ortiz., A. Pandolfi, “Three-dimensional finite-element simulation of the dynamic Brazilian test on concrete cylinders”, *Int.J. Numer. Meth. Engng*., 48, pp.963-994, 2000.

[4] K.Raoufi, M. Pour-Ghaz, A. Poursaee, J. Weiss, “Restrained shrinkage cracking in concrete elements: The role of substrate bond on crack development”, *Journal of Materials in Civil Engineering*, accepted manuscript, 2010.

[5] M.D.C. Ferreira, W.S. Venturini, F. Hild, “On the analysis of notched concrete beams: From measurement with digital image correlation to identificaciont with boundary method of a cohesive model”, *Engineering Fracture Mechanics*, 78, pp. 71-84, 2011.

[6] X.Hu, F.H. Wittmann, “Experimental method to determine extension of the fracture process zone”, *Journal of Materials in Civil Engineering*, 2(1), 1990.

[7] ASTM C 192. “Standard practice for making and curing concrete test specimens in the laboratory”.

[8] R.John, S.P.Shah, “Fracture mechanics analysis of high-strength concrete”, *Journal of Materials in Civil Engineering*, 1(4), 1989.

[9] D. S. Dugdale, “Yielding of steel sheets containing slits”, *J. Mech. Phys. Solids*, 8, pp. 100–104, 1960.

[10] G.I. Barenblatt, “The mathematical theory of equilibrium cracks in brittle fracture”, *Advances in Applied Mechanics*, 7, pp. 55–129, 1962.

[11] V. Tvergaard, J.W. Hutchinson, “The relation between crack growth resistance and fracture process parameters in elastic-plastic solids”, *J. Mech. Phys. Solids*, 40, pp. 1377–1397, 1992.

[12] X.-P. Xu, A. Needleman, “Numerical simulations of fast crack growth in brittle solids”, *J. Mech. Phys. Solids*, 42(9), pp. 1397–1434, 1994.

[13] G. Camacho, M. Ortiz, “Computational modeling of impact damage in brittle materials”, *Int. J. Solids Structures*, 33(20-22), pp. 2899–2938, 1996.

[14] H.D. Espinosa, P.D. Zavattieri. “A grain level model for the study of failure initiation and evolution in polycrystalline brittle materials. Part I: Theory and numerical implementation”. *Mechanics of Materials*, 35, pp. 333-364, 2003.

[15] J.W. Morrissey, J.R. Rice. “Crack front waves”, *J. Mech. Phys. Solids*, 46(3), 467-487, 1998.

[16] M.L. Falk, A. Needleman, J.R. Rice , “A critical evaluation of cohesive zone models of dynamic fracture”, Proceedings of the 5th European mechanics of materials conference on scale transitions from atomistics to continuum plasticity, 11, pp. 43-50, 2001.

[17] J.R. Rice, “The Mechanics of earthquake rupture, Physics of the Earth’s Interior” (Proc. Int’l School of Physics ‘Enrico Fermi,’ ed. A.M. Dziewonski and E. Boschi), North-Holland, 555-649, 1980.

[18] J.C.A.M. van Doormaal, J.Weerheijm, L.J. Sluys, “Experimental and numerical determination of the dynamic fracture energy of concrete”, *Journal de Physique*, 4, 1994.

[19] R.E. Roelfstra, F.H. Wittmann, “A numerical method to link strain softening with fracture in concrete, Fracture Toughness and Fracture Energy in Concrete”, edited by F.H. Wittmann, Elsevier Science, pp. 163-175, 1986.